



Effect of polyaniline particle size on the chromate adsorption from aqueous electrolyte

Nesrine Allal¹ · Abderrezak Abdi¹ · Radia Bagtache² · Mohamed Trari³

Received: 30 May 2024 / Revised: 19 August 2024 / Accepted: 31 August 2024

© The Author(s), under exclusive licence to Springer-Verlag GmbH Germany, part of Springer Nature 2024

Abstract

In this contribution, we report the investigation on removing of the oxochromium (VI), a hazardous species, using HCl-doped polyaniline (PAni-HCl) as adsorbent versus particles size. PAni-HCl has been successfully elaborated by conventional oxidative chemical method in the temperature range (0–3 °C). The recovered powder was milled and sieved into size ranges of < 50, 50–63, 125–160 and > 200 μm. The batch adsorption experiments were performed at 25 °C, using 250 mg of PAni-HCl dispersed in 250 mL of Cr(VI) aqueous solution (250 mg L⁻¹). The Cr(VI) uptake was significantly influenced by both the particle size and contact time. Smaller particle sizes allow a quick initial adsorption and high removal efficiency (~100%). The kinetics of the Cr(VI) adsorption follow the pseudo-second-order model. A good correlation was demonstrated between the removal chromium (VI) properties ($Q_{e,exp}$, k_2 and $\tau(\%)$) and the (normalized) mean diameter ratio.

Keywords Chromium (VI) sorption · Polyaniline · Removal efficiency · Pseudo-second-order kinetic model · Powder

Introduction

Among various conducting polymers, polyaniline has been widely studied because of its facile synthesis and its good chemical stability both in air [1, 2] and acidic media over a large pH range. Polyaniline has been used in many

✉ Mohamed Trari
solarchemistry@gmail.com; bagtacheradia@yahoo.fr

¹ Laboratory of Electrochemistry and Corrosion, Ecole Militaire Polytechnique, BP17, 16000 Algiers, Algeria

² Laboratory of Electrochemistry-Corrosion, Metallurgy and Inorganic Chemistry, Faculty of Chemistry, USTHB, BP 32, 16111 Algiers, Algeria

³ Laboratory of Storage and Valorization of Renewable Energies, Faculty of Chemistry, USTHB, BP32, 16111 Algiers, Algeria

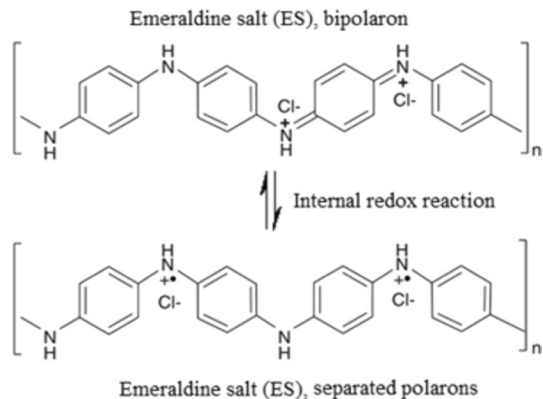
applications such as dye-sensitized solar cells [3], hydrogen photoproduction [4], corrosion protection [5], gas sensors [6], glucose biosensor [7], the removal of pharmaceutical drugs [8] as well as the storage and conversion of energy [9].

The polymers family is versatile system with general formula: $[(-B-NH-B-NH-)_y(-B-N=Q=N-)_{1-y}]_n$ [10]; B and Q denote the rings C_6H_4 in the benzenoid and the quinoid forms, respectively. The fully reduced leucoemeraldine base polymer (LEB; $y = 1$), the fully oxidized pernigraniline base polymer (PB; $y = 0$), the halfoxidized form emeraldine base (EB; $y = 0.5$) and 75% intrinsically oxidized nigraniline (NA; $y = 0.75$) are all insulators. On the contrary, the protonation of the EB form produces the polaronic or bipolaronic emeraldine salt (ES) (Fig. 1), with a high conductivity ($\sim 2-10 \text{ S cm}^{-1}$) [10-12].

Many reports have been devoted to polyaniline as an adsorbent for removing heavy metals and chromium (VI) in particular [13-19]. Nevertheless, to our knowledge, no studies have been reported on the effect of polyaniline particle size on the removal efficiency of chromium (VI) before now.

Chromium belongs to the category of heavy metals that are potentially hazardous for the human health and environment even at very low concentration [20]. In waste aqueous systems, it exists mainly in two oxidation states, trivalent, Cr (III) and hexavalent, Cr(VI) states. The later variety is considered the most toxic by both the World Health Organization (WHO) and the Environmental Protection Agency (EPA) due to its carcinogenicity and mutagenicity on humans [21, 22]. The US Environmental Protection Agency (USEPA) established for the total chromium content (III and VI) that the maximum contaminant level (MCL) was 0.1 mg/L, due to the possible Cr(III)-Cr(VI) inter-conversions, depending on environmental conditions [23]; however, a level of 0.05 mg/L of chromium (VI) has been retained as a provisional guideline value by the WHO [24]. In this work, we investigate a relationship between the polyaniline particles size (PS) and the chromium (VI) sorption efficiency. This is done to enrich the literature on polyaniline where the adsorption properties have not been fully investigated.

Fig. 1 The protonated emeraldine salt forms (PANI-ES)



Experimental

All products were supplied by the Alfa Aesar Company with purity greater than 99%, and solutions were prepared in deionized water. Polyaniline doped with HCl (PAni-HCl) has been prepared by a typical oxidation method using ammonium peroxodisulfate ((NH₄)₂S₂O₈) in aqueous acidic media (HCl) [24].

Initially, 0.055 mmol of aniline (~5 mL) was dissolved in 100 mL of HCl solution (1 M) in volumetric flask, then 150 mL of solution containing the oxidized agent (NH₄)₂S₂O₈ (0.063 mmol) was added dropwise to the solution containing the aniline monomer. The molar ratio [S₂O₈²⁻]/[C₆H₅NH₂] was taken to be 1.15. The mixture was left under stirring for 8 h at a temperature in the range (0–3°C), using an ice bath. The dark green precipitate was recovered by vacuum filtration and washed several times with both distilled water and acetone, and finally dried under reduced pressure in an oven for 72 h. The obtained powder was milled using an IKA laboratory mill (M20, Werke Staufen, Germany) for then sieved (30 min) using a FRITTSCH vertical vibratory sieve shaker (model Analysette 3 PRO, Germany) into size ranges of < 50, 50–63, 125–160 and > 200 μm. Finally, the powders were placed in desiccators until use.

The X-ray diffraction (XRD) data were recorded with a PANalytical X'Pert PRO diffractometer (CuK_α radiation, λ = 1.54056 Å) over 2θ range (3–60°) with an increment of 0.008° and a scanning rate of 0.1° min⁻¹. The morphology and particle size were determined with a QUANTA 250 Scanning Electron Microscope (LV-SEM). The Fourier transform infrared (FTIR) analysis was performed using a Shimadzu spectrophotometer equipped with a DTGM KBr detector. The particle size analysis was performed by dry mode (at 1 bar), according to Mie theory, using a CILAB 1190DL Laser Particle Size Analyzer.

The sorption experiments were performed in a double-walled Pyrex reactor (500 cm³ capacity). A 250 mg of PAni-HCl powder was added to 250 mL of Cr₂O₇²⁻ solution (250 mg L⁻¹, pH~4.5). The sorbent powder was dispersed by vigorous stirring (500 rpm), and the temperature was set at 25 °C thanks to a thermostat (LAUDA E10 S). Samples of 1 mL were drawn at 0, 0.5, 1, 2, 5, 10, 20, 40 and 60 min using a syringe with FTFE filter and then were diluted to 10 mL with deionized water in appropriate volumetric flasks.

The residual chromium concentration was evaluated in the λ-range (200–370 nm), using a UV-2401 Shimadzu spectrophotometer. The calibration curve (slope = 0.015 mg⁻¹ L, R² = 0.998) was performed using samples with Cr(VI) concentrations in the range (1–50 mg/L). The adsorption capacity (Q_t, mg g⁻¹) and the removal efficiency (τ, %) are calculated using Eqs. (1) and (2):

$$Q_t (\text{mg g}^{-1}) = \{[\text{Cr(VI)}]_0 - [\text{Cr(VI)}]_t / m\} \times V \quad (1)$$

$$\tau (\%) = \{[\text{Cr(VI)}]_0 - [\text{Cr(VI)}]_e / [\text{Cr(VI)}]_0\} \times 100 \quad (2)$$

where [Cr(VI)]₀, [Cr(VI)]_t and [Cr(VI)]_e are the initial, at time *t* and equilibrium concentrations (mg L⁻¹) of the chromium (VI); *V* and *m* are the volume of the solution and the mass of polyaniline adsorbent (*g*).

Results and interpretation

Material characterization

Figure 2 shows a typical X-ray diffraction pattern of a semi-crystalline PANi-HCl structure. All peaks are assigned to the monoclinic unit cell (space group: $P2_1$), in agreement with the literature data [25, 26]. Furthermore, the broad peaks at ~ 20 and 25° are attributed, respectively, to the periodicity parallel and perpendicular to the ES chains [27]. The main vibration peaks identifying the chemical structure of polyaniline are shown in the FTIR-ATR spectra (Fig. 3). The peaks at 794 and 1101 cm^{-1} are attributed to the C–H out-of-plane deformation in the 1,4-disubstituted benzene ring, and aromatic C–H in-plane stretching vibration, respectively [28, 29]. The absorption peaks 1240 and 1292 cm^{-1} are ascribed to the C–N⁺ frequency mode of the polaronic lattice and to the C–N vibration in benzenoid ring, respectively [30]. Moreover, the peaks 1468 and 1651 cm^{-1} are assigned to the C=C stretching deformation in the sequencing of benzenoid and quinoid units, respectively [31]. Furthermore, the peak at 3440 cm^{-1} belongs to the stretching vibration of the CN groups.

The SEM image (Fig. 4) shows a non-uniform and porous microstructure based on highly agglomerate particles. This morphology offers more favorable adsorption sites compared to a compact surface and seems to have an appreciable potential for retaining Cr(VI) ions.

Particle size analysis

The particle size distributions (PSD) are obtained in terms of cumulative and frequency semi-logarithmic plots except for particles sizes smaller than $50\text{ }\mu\text{m}$ (Fig. 4, Inset), the distributions are multimodal (multiple peaks). All the most intense peaks are wide and non-symmetric (left and right-skewed) indicating polydispersed particles. For a

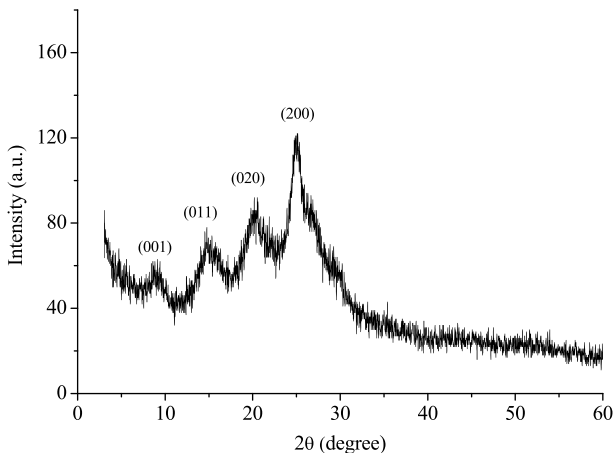


Fig. 2 XRD pattern of prepared material

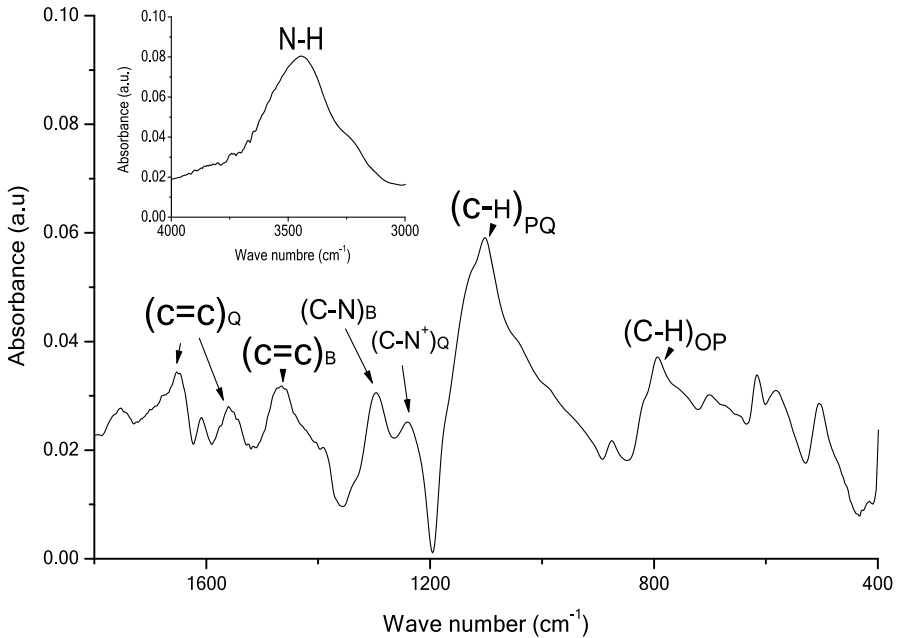


Fig. 3 FTIR infrared spectra of the elaborated material

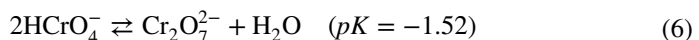
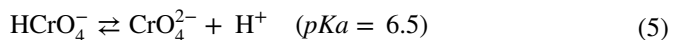
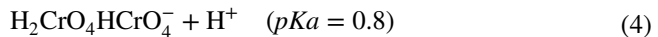
non-symmetrical distribution and large particles, its more accurate to report the volume weighted mean diameter $D_{4,3}$, given by equation (3) [32, 33]:

$$D_{4,3} = \left(\sum n_i D_i^4 \right) / \left(\sum n_i D_i^3 \right) \quad (3)$$

where n_i is the number-based frequency of particles in the same class i , having the mean diameter D_i . All $D_{4,3}$ values are presented in Table 1.

Chromium (VI) speciation

According to the Cr(VI) predominance diagram (at 25 °C) [34, 35], the pH affects the significantly the chemical equilibrium involving both the $H_2CrO_4-Cr_2O_7^{2-}-CrO_4^-$ or $H_2CrO_4-HCrO_4^- -CrO_4^-$ systems, depending on the total chromium concentration (TCC); all species are linked by the following acid–base equilibriums [13, 34]:



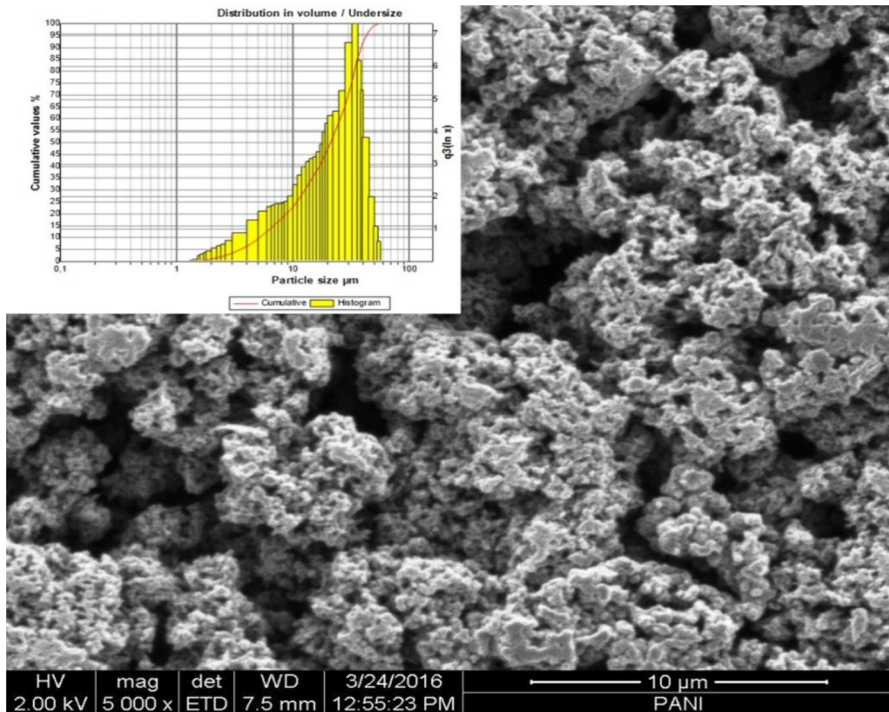


Fig. 4 SEM micrograph of the recovered powder. Inset: The particle size distribution of the powder with small size range (<50 μm)

Table 1 Particle size specifications and removal properties

Property	< 50 μm	50–63 μm	125–160 μm	200–500 μm
<i>Particle size specifications</i>				
$D [3, 4]$ (μm)	21.86	49.53	155.7	267.6
Mode (μm)	36.00	53.00	160.0	300.0
<i>Removal properties</i>				
τ (%)	98.72	95.80	87.88	77.36
$Q_{e,exp}$ (mg/g)	246.8	239.5	224.0	191.6
k_2 (mg g ⁻¹ min ⁻¹ × 10 ²)	1.824	0.582	0.145	0.099
$Q_{e,cal}$ (mg/g)	247.5	242.1	238.1	210.1
Slope (g mg ⁻¹ × 10 ³)	4.04	4.13	4.20	4.76
R^2	0.999	0.999	0.993	0.980

In the pH range (2–6), Cr(VI) exists as dichromate $Cr_2O_7^{2-}$ or as bichromate $HCrO_4^-$, depending on TCC less or higher than $10^{-1.68}$ mol/L (pCr=1.68). Nevertheless, at pH 4.5 and TCC of 2.157×10^{-3} M (pCr=2.66), the Cr(VI) species are mainly present in the form of $HCrO_4^-$, and therefore, the $H_2CrO_4-HCrO_4^- - CrO_4^{2-}$ system is considered in our study with TCC given by (7):

$$[\text{Cr(VI)}]_{\text{TCC}} = [\text{H}_2\text{CrO}_4] + [\text{HCrO}_4^-] + [\text{CrO}_4^{2-}] \quad (7)$$

Spectrophotometry

The residual chromate Cr(VI) concentration versus time was evaluated by UV–visible spectrophotometry. Figure 5 gives the absorption spectra of residual Cr(VI) samples. The two intense peaks at 350 nm ($28,571 \text{ cm}^{-1}$) and 274 nm ($36,496 \text{ cm}^{-1}$) are attributed to $2t_{1u}-e_g$ and $2t_{1u}-t_{2g}$ transitions, respectively. It is well known that the inter-bands electronic charge transfer in both tetrahedral complexes $\text{Cr}_2\text{O}_7^{2-}$ and CrO_4^{2-} occurs between the higher occupied oxygen anti-bonding $2p^*(\text{O}^{2-})$ molecular orbital and the unoccupied chromium non-bonding e_g and t_{2g} of $3d$ (Cr^{7+}) molecular orbital. The $2p^*-3d$ transitions are classified as ligand-to-metal charge transfer (LMCT) and are spin and Laporte allowed [36].

The spectrograms clearly exhibit the effect of the polyaniline particles size on the amount of Cr(VI) adsorbed. Indeed, the optical density abruptly decreases for grain sizes less than $50 \mu\text{m}$, while it gradually decreases for particle sizes $> 200 \mu\text{m}$ (Fig. 5, Inset).

The mechanism of the Cr(VI) removal was described by many authors [16, 17, 37] as chelate-type interactions between the imine and amine functional groups of the polyaniline particles and the negatively charged chromium species, which is

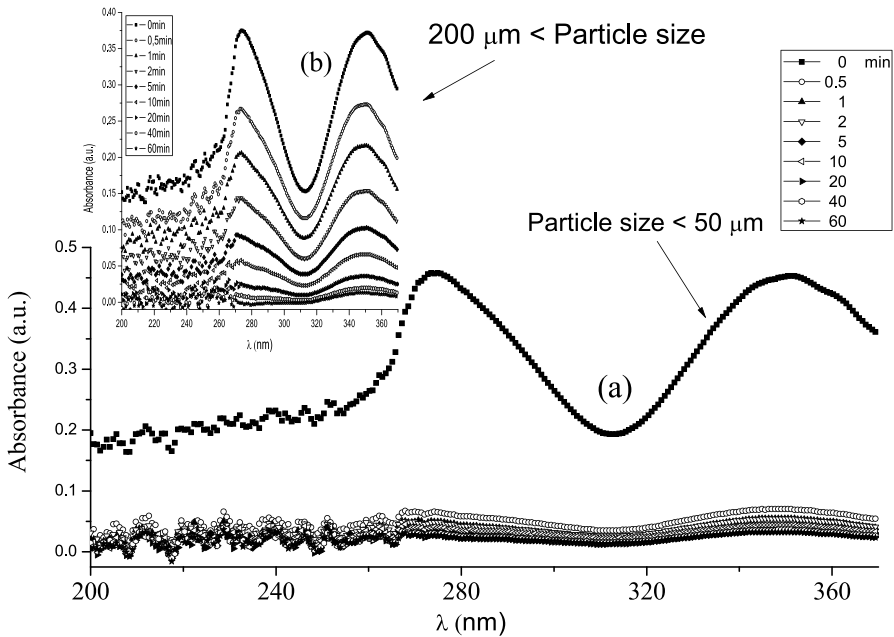
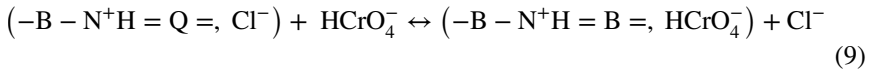
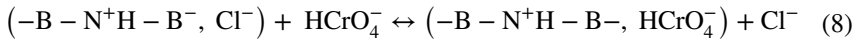


Fig. 5 UV–Vis absorption spectra of residual Cr(VI) solutions versus the contact time with particles sizes of: **a** $< 50 \mu\text{m}$ and **b** $> 200 \mu\text{m}$

pH-dependent. In parallel to the electrostatic interactions, a fraction of Cr(VI) is reduced to Cr(III).

The adsorption of the predominating form HCrO_4^- on protonated PANi-HCl particles occurs simultaneously with releasing Cl^- ions, through an ion-exchange process. Therefore, we suggest mechanism according to Eqs. (8) and (9), in agreement with ref. [38, 39]:



Effect of contact time and particle size

The evolutions of [Cr(VI)] versus contact time for different adsorbent particle sizes (<50, 50–63, 125–160 and >200 μm) are illustrated in Fig. 6. The batch adsorption experiments were conducted at 25 °C for 60 min, with an initial concentration of 250 mg L⁻¹ and polyaniline adsorbent dose of 1 g/1000 mL. The figure reveals that the uptake is significantly influenced by both the particle size and contact time; the latter clearly enhanced the percent removal of Cr(VI).

In addition, under the same experimental conditions, powder with small particle size allows both rapid and significantly improved absorption. Indeed, for the first 30 s, more than 80% of Cr(VI) was removed using small sizes particles (<50 μm), in contrast with those of >200 μm where only 14% was eliminated.

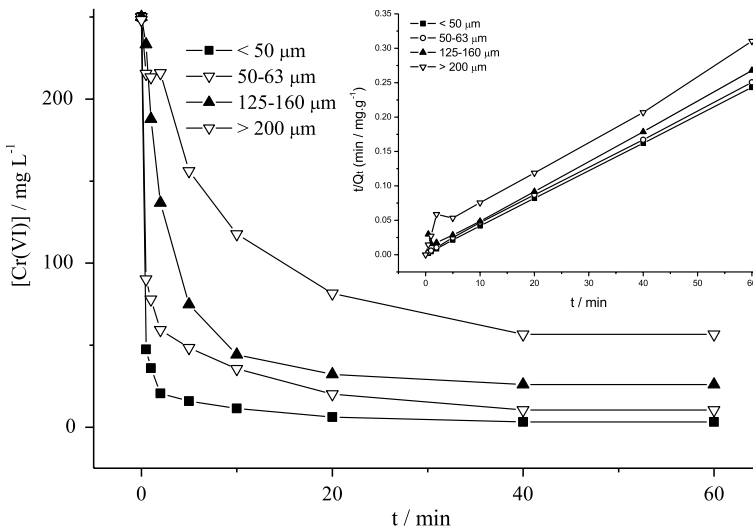


Fig. 6 Effect of the particle size and contact time on the Cr(VI) removal. Inset: Kinetic of pseudo-second order. Initial Cr(VI) concentration = 250 mg L⁻¹; pH 4.5; T = 298 K

For both particle sizes $< 50 \mu\text{m}$ and $> 200 \mu\text{m}$, the equilibrium was reached after 40 min, and the calculated uptake efficiencies were found to be 99 and 77%, respectively. Such results are due to the enhanced external surface absorption, and hence to increase the number of adsorption sites. It is well established now that both physical and chemical phenomena are strongly influenced by the size and geometry of the materials [40, 41]; they become more pronounced as the particles size decreases, and the surface area-to-volume ratio increases [42].

Adsorption kinetic study

Throughout the studied particle sizes range, the linear plots t/Q_t versus time (t) illustrated in Fig. 6, Inset, indicate that the Cr(VI) adsorption follows a pseudo-second-order (PSO) model, given by [43]:

$$t/Q_t = \{1/K_2 Q_e^2 + t/Q_e\} \tag{10}$$

where k_2 ($\text{mg g}^{-1} \text{min}^{-1}$) is the rate constant of pseudo-second-order adsorption, Q_e (mg g^{-1}) and Q_t (mg g^{-1}) the adsorbed amounts at equilibrium at time t . The values of Q_e and k_2 are evaluated, respectively, from the slope and the intercept of the straight lines.

According to Ho and Mckay, the adsorption kinetics obeying to the PSO model mainly occurs by means of chemisorption, through an electronic exchange between the adsorbate species Cr(VI) and the adsorption sites [44].

The kinetic parameters of PSO are listed in Table 1. The correlation coefficient (R^2) was found to be close to unity, revealing the good correlation for the Cr(VI) HCrO_4^- adsorption of on polyaniline particles. The PSO model is verified for a linear regression coefficient $R^2 \geq 0.9$ [44]. In addition, for particles with small sizes, the experimental and theoretical values of $Q_{e,\text{exp}}$ and $Q_{e,\text{cal}}$ were found to be close to each other.

Figures 7 and 8 show, respectively, the variation of the adsorption capacity and the removal efficiency versus the inverse of the diameter ratio $D_{4,3}^{-1}$, normalized to $D_{4,3}$ of particles with size range $> 200 \mu\text{m}$. The experimental data are well fitted by using, respectively, the trend lines:

$$Q_{e,\text{exp}} (\text{mg g}^{-1}) = -59.83 x (D_{4,3})^{-1} + 252.3 (R^2 = 0.965) \tag{11}$$

$$\tau (\%) = -23.57 \times (D_{4,3})^{-1} + 100.5 (R^2 = 0.996) \tag{12}$$

Figure 8, insert, reveals a clear linear relationship between the rate constant and the (normalized) diameter ratio. In fact, the obtained data are well-fitted using a linear model according to the trend line:

$$K_2 (\text{mg g}^{-1} \text{min}^{-1}) = 0.15 (D_{4,3}) - 0.128 (R^2 = 0.981) \tag{13}$$

The regression coefficients indicate a strong correlation between all the properties obtained and the average diameter ratio $D_{4,3}$, over a grain size range (20–300 μm).

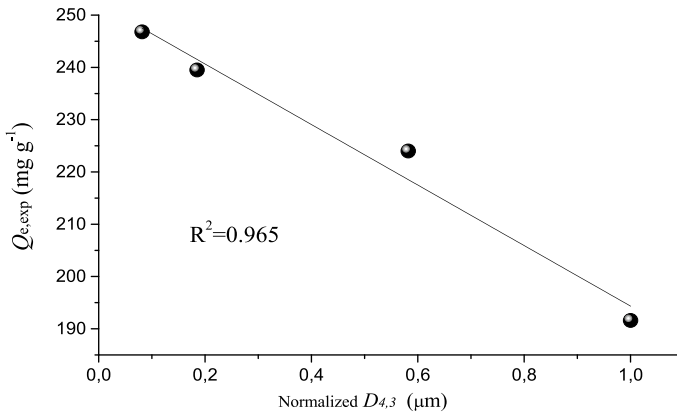


Fig. 7 Adsorption capacity versus the mean diameter $D_{4,3}$

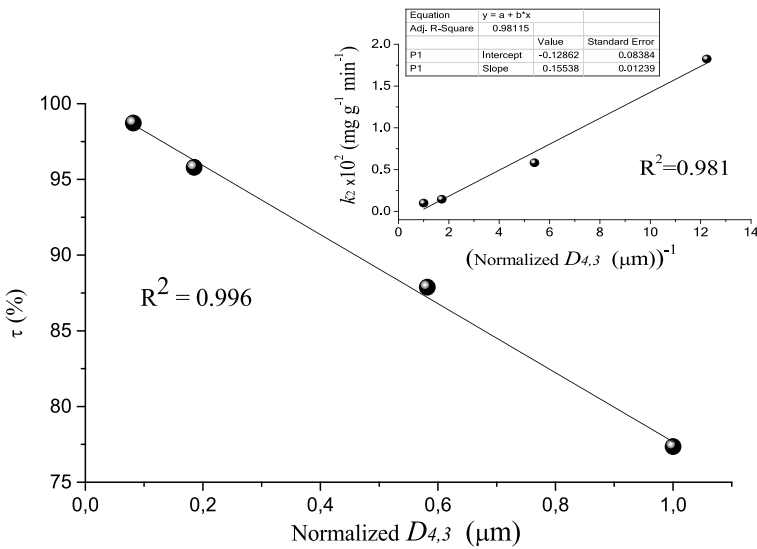


Fig. 8 The Cr(VI) removal efficiency versus the mean diameter $D_{4,3}$. Insert: the rate constant versus the inverse of the mean diameter

Therefore, it can be seen that the smaller the particles of the adsorbent, the faster the adsorption process and the greater the amount of Cr(VI) removed.

The relationship of the proportionality was highlighted in the previous works [45–48]. In fact, Krishna [46] has studied the effect of the particles size (PS=0.6, 0.8 and 1.7 mm) on the adsorption kinetics for removing Cr(VI) species media using calcined brick powder as adsorbent. He has attributed the increase in the adsorption capacity using smaller particles to both the greater accessibility to pores and a larger surface area for the bulk adsorption. Shanmugam et al. [48] have given the same explanation after studying the sorption of Cibacron blue F3GA using

Table 2 Cr(VI) adsorption capacities of the previous works

Adsorbent	Equilibrium time (min)	pH	<i>T</i> (K)	Adsorption capacity (mg/g)	References
Polyaniline-coated ethyl cellulose	30	1.0	303	38.76	[49]
Kapok fiber–polyaniline	60	3.7–6.6	300	44.05	[13]
Magnetic mesoporous carbon–polyaniline	120	2.0	298	172.33	[16]
Poly(2-ethylaniline)/chitosan	240	3.0	298	147.16	[50]
Polyaniline/polyvinyl alcohol	60	4.0		1112.3	[51]
Calcined brick powder	60	2.0	300	200	[46]
PEI-modified magnetic adsorbent	30	2.0	298	78.13	[52]
Modified magnetic mesoporous silica MCM-48	90	4.0	298	115.60	[53]
Amino-functionalized mesoporous alumina	60	2.0	298	59.50	[54]
Polyaniline (<50 μm)	40	4.5	298	246.8	This study
Polyaniline (200–500 μm)	40	4.5	298	191.6	

a spirulina platensis biomass as adsorbent, with an increases in particle sizes from <75 to >600 μm. They indicate that the particles with smaller sizes improve the availability of the surface area and consequently the number of binding sites.

The uptake capacities have been compared with those of other adsorbents for the removal of Cr(VI) (Table 2), and it is clearly seen that PAni-HCl exhibits an interesting potential as adsorbent for removing heavy metals, particularly when the uptake is undertaken using small size particles.

Conclusion

In summary, HCl-doped polyaniline was prepared by chemical route at low temperature (0–3° C). The XRD pattern reveals a typical semi-crystalline structure. The SEM characterization showed a non-uniform and porous microstructure based on highly agglomerate particles, offering more adsorbing sites and higher uptake performance. The recovered powder was crushed and sieved into size ranges <50, 50–63, 125–160 and >200 μm. The particle sizes analysis indicated a multimodal distributions, except for <50 μm. The residual [Cr(VI)] versus time plots revealed that the small particle sizes give both fast and efficient metal removal, approaching ~100% efficiency. The adsorption follows a pseudo-second-order model. Inverse linear relationships were demonstrated between adsorption capacity and removal efficiency relative to the mean (normalized) diameter ratio, unlike the rate constant k_2 for which the experimental data are well fitted using a linear model.

Acknowledgement The financial support of this work was supported by the University of Boumerdes (UMBB, Algeria).

Author Contribution N. A. helped in experimentation; A. A. helped in conception and writing the draft manuscript; R. B. helped in methodology and software and M. T. helped in revision and supervision of the final version.

Data availability All data generated in this work are analyzed in this work are included in the submitted article.

Declarations

Conflicts of interest The authors declare no competing interests.

References

- Samadi A, Xie M, Li J, Shon H, Zheng C, Zhao S (2021) Polyaniline-based adsorbents for aqueous pollutants removal: a review. *Chem Eng J* 418(15):129425
- Nguyen VH, Lamiel C, Kharismadewi D, Tran VC, Shim J-J (2015) Covalently bonded reduced graphene oxide/polyaniline composite for electrochemical sensors and capacitors. *J Electroanal Chem* 758:148–155
- Dwivedi G, Munjal G, Bhaskarwar AN, Chaudhary A (2022) Dye-sensitized solar cells with polyaniline: a review. *Inorg Chem Commun* 135:109087
- Belabed Ch, Abdi A, Benabdelghani Z, Rekhila G, Ettxeberria A, Trari M (2013) Photoelectrochemical properties of doped polyaniline: application to hydrogen photoproduction. *Int J Hydrogen Energy* 38:6593–6599
- Gao F, Mu J, Bi Z, Wang S, Li Z (2021) Recent advances of polyaniline composites in anticorrosive coatings: a review. *Prog Org Coat* 151:106071
- Fratoddi I, Venditti I, Cametti C, Russo MV (2015) Chemiresistive polyaniline-based gas sensors: a mini review. *Sens Actuators B Chem* 220:534–548
- Lai J, Yi Y, Zhu P, Shen J, Wu K, Zhang L, Liu J (2016) Polyaniline-based glucose biosensor: a review. *J Electroanal Chem*, 782 (<https://www.sciencedirect.com/journal/journal-of-electroanalytical-chemistry/vol/782/suppl/C2016>) 138–153
- Higgins P, Siddiqui SH (2022) Efficacy of polyaniline (PANI) nanofibres for capturing diclofenac (DC) drug from its aqueous solutions. *J Indian Chem Soc.* <https://doi.org/10.1016/j.jics.2022.100494>
- Duan X, Deng J, Wang X, Guo J, Liu P (2016) Manufacturing conductive polyaniline/graphite nanocomposites with spent battery powder (SBP) for energy storage: a potential approach for sustainable waste management. *J Hazardous Mater* 312:319–328
- Ayad MM, Sheneshin MA (2004) Effect of acids on in situ polyaniline film formation. *Polym Int* 53(8):1180–1184
- Bernard MC, Hugot-Le Goff A (2006) Quantitative characterization of polyaniline films using Raman spectroscopy I: polaron lattice and bipolaron. *Electrochim Acta* 52(2):595–603
- Zujovic ZD, Zhang L, Bowmaker GA, Kilmartin PA, Travas-Sejdic J (2008) Self-assembled, nanostructured aniline oxidation products: a structural investigation. *Macromolecules* 41:3125–3135
- Tripathy S, Sahu S, Kishore Patel R, Bihari Panda R, KumarKar P (2021) Efficient removal of Cr(VI) by polyaniline modified biochar from date (*Phoenix dactylifera*) seed. *Groundw Sustain Devt* 15:100653
- Li R, Liu L, Yang F (2014) Removal of aqueous Hg(II) and Cr(VI) using phytic acid doped polyaniline/cellulose acetate composite membrane. *J Haz Mater* 280:20–30
- Eskandari E, Kosari M, Farahani MHDA, Khiavi ND, Saeedikhani M, Katal R, Zarinejad M (2020) A review on polyaniline-based materials applications in heavy metals removal and catalytic processes. *Sep Purif Technol* 231(16):115901
- Wang J, Zhang K, Zhao L (2014) Sono-assisted synthesis of nanostructured polyaniline for adsorption of aqueous Cr(VI): effect of protonic acids. *Chem Eng J* 239:123–131
- Herath A, Reid C, Perez F, Pittman CU Jr, Mlsna TE (2021) Biochar-supported polyaniline hybrid for aqueous chromium and nitrate adsorption. *J Environ Manage* 296:113186

18. Senguttuvan S, Senthilkumar P, Janaki V, Kamala-Kannan S (2021) Significance of conducting polyaniline based composites for the removal of dyes and heavy metals from aqueous solution and wastewaters: a review. *Chemosphere* 267:129201
19. Rajapaksha AU, Selvasembian R, Ashiq A, Gunarathne V, Ekanayake A, Perera VO, Wijesekera H, Mia S, Ahmad M, Vithanage M, SikOk Y (2022) A systematic review on adsorptive removal of hexavalent chromium from aqueous solutions: recent advances. *Sci Total Environ* 809(25):152055
20. Ukhurebor KE, Aigbe UO, Onyancha RB, Nwankwo W, Osibote OA, Paumo HK, Ama OM, ADETUNJI CO, Siloko IU (2021) Effect of hexavalent chromium on the environment and removal techniques: a review. *J Environ Manage* 280(15):111809
21. IARC (2012) Arsenic, metals, fibres and dusts volume 100 C A review of human carcinogens. International Agency for Research on Cancer, World Health Organization, Lyons
22. U.S. Environmental Protection Agency (USEPA) (2016) Chromium in drinking water. <https://www.epa.gov/dwstandardsregulations/chromium-drinking-water>
23. WHO (2003) Chromium in drinking-water: background document for development of WHO guidelines for drinking-water quality. World Health Organization, Geneva
24. Rao PS, Subrahmanya S, Sathyanarayana DN (2002) Inverse emulsion polymerization: a new route for the synthesis of conducting polyaniline. *Synth Met* 128(3):311–316
25. Moon YB, Cao Y, Smith P, Heeger AJ (1989) X-ray scattering from crystalline polyaniline. *polymer. Communications* 30:196–199
26. Kar P, Choudhry AR (2013) Carboxylic acid functionalized multi-walled carbon nanotube doped polyaniline for chloroform sensors. *Sensor Actuat B* 183:25–33
27. Zhao W, Ma L, Lu K (2007) Facile synthesis of polyaniline nanofibers in the presence of polyethylene glycol. *J Polym Res* 14:1–4
28. Kang ET, Neoh KG, Tan KL (1998) Polyaniline: a polymer with many interesting intrinsic redox states. *Prog Polym Sci* 23:277–324
29. Palaniappan S (2001) Chemical and electrochemical polymerization of aniline using tartaric acid. *Eur Polym J* 37(5):975–981
30. Li X, Ju M, Li X (2004) Chlorine ion sensor based on polyaniline film electrode. *Sensor Actuat B* 97:144–147
31. Jiang N, Xu Y, Dai Y, Luo W, Dai L (2012) Polyaniline nanofibers assembled on alginate microsphere for Cu²⁺ and Pb²⁺ uptake. *J Haz Mater* 215:17–24
32. Allen T (1992) Particle size measurement, 4th edn. Chapman & Hall, London
33. Henk G (2009) Merkus particle size measurements: fundamental, practice, quality. Springer, New York
34. Pourbaix M (1974) Atlas of electrochemical equilibria in aqueous solutions. Pergamon Press, Oxford
35. Pouloupoulou VG, Vrachnou E, Koinis S, Katakis D (1997) The Cr2O7²⁻–CrO4²⁻–HCrO4⁻ system revised. *Polyhedron* 16(3):521–524
36. Burkov VI, Egorysheva AV, Kargin YuF (2003) Electronic structure and optical spectra of tetrahedral [MO₄]ⁿ⁻ complexes of 3d metals. *Russ J Inorg Chem* 48(4):537–555
37. Phan TB, Do NQ, Mai TTT (2010) Preparation of cellulose nanocrystal-based poly (m-aminobenzene sulfonate) copolymer for heavy metal Cr (VI) adsorption. *Adv Nat Sci Nanosci Nanotechnol* 1(035006):1
38. Ebrahim S, Shokry A, Ibrahim H, Soliman M (2016) Polyaniline/akaganéite nanocomposite for detoxification of noxious Cr(VI) from aquatic environment. *J Polym Res* 23:79
39. Davis ME, Davis RJ (2003) Fundamentals of chemical reaction engineering, 1st edn. McGraw-Hill, New-York
40. Chaturvedi S, Dave PN, Shah NK (2012) Applications of nano-catalyst in new era. *J Saudi Chem Soc* 16:307–325
41. Liu Y, Zhao G, Wang D, Li Y (2015) Heterogeneous catalysis for green chemistry based on nanocrystals. *Natl Sci Rev* 2:150–166
42. Hoa Y-S, Ofomaja AE (2006) Pseudo-second-order model for lead ion sorption from aqueous solutions onto palm kernel fiber. *J Haz Mater B* 129:137–142
43. Li Z, Ye BA, Hu X, Ma X, Zhang X, Deng Y (2009) Facile electropolymerized-PANI as counter electrode for low cost dye-sensitized solar cell. *Electrochem Commun* 11:1768–1771
44. Ho YS (2006) Second-order kinetic model for the sorption of cadmium onto tree fern: a comparison of linear and non-linear methods. *Water Res* 40(1):119–125

45. Kannan N, Pagutharivalan R (2012) Removal of Congo red from aqueous media by adsorption using eucalyptus globules bark carbon as an adsorbent. *EJEAF Chem* 11(4):358–374
46. HemaKrishna R, Swamy AVS (2012) Investigation on the effect of particle size and adsorption kinetics for the removal of Cr (VI) from the aqueous solutions using low cost sorbent. *Eur Chem Bull* 1(7):258–262
47. Wong YC, Szeto YS, Cheung WH, McKay G (2008) Effect of temperature, particle size and percentage deacetylation on the adsorption of acid dyes on chitosan. *Adsorption* 14–1:11–20
48. Shanmugam D, Alagappan M, Rajan RK (2016) Bench-scale packed bed sorption of Cibacron blue F3GA using lucrative algal biomass. *Alex Eng J* 55(3):2995–3003
49. Guo X, Fei GT, Su H, Zhang LD (2011) *J Phys Chem C* 115:1608–1613
50. Yavuz AG, Dincturk-Atalay E, Uygun A, Gode F, Aslan E (2011) *Desalination* 279:325–331
51. Karthik R, Meenakshi S (2015) Adsorption study on removal of Cr(VI) ions by polyaniline composite. *Desalin Water Treat* 54(11):3083–3093
52. Pang Y, Zeng GM, Tang L, Zhang Y, Liu YY, Lei XX, Li Z, Zhang JC, Liu ZF, Xiong YQ (2011) Effective removal of Cr(VI) from aqueous solution based on APTES modified nanoporous silicon prepared from kerf loss silicon waste. *Chem Eng J* 175:222–227
53. Anbia M, Kargosha K, Khoshbooei S (2015) Heavy metal ions removal from aqueous media by modified magnetic mesoporous silica MCM-48. *Chem Eng Res Des* 93:779–788
54. Cai WQ, Tan LJ, Yu JG, Jaroniec M, Liu XQ, Cheng B, Verpoort F (2014) *Chem Eng J* 239:207–215

Publisher's Note Springer Nature remains neutral with regard to jurisdictional claims in published maps and institutional affiliations.

Springer Nature or its licensor (e.g. a society or other partner) holds exclusive rights to this article under a publishing agreement with the author(s) or other rightsholder(s); author self-archiving of the accepted manuscript version of this article is solely governed by the terms of such publishing agreement and applicable law.